Estimation of the Atmospheric Flux of Nutrients and Trace Metals to the Eastern Tropical North Atlantic Ocean*

C. F. POWELL

Centre for Ocean and Atmospheric Sciences, School of Environmental Sciences, University of East Anglia, Norwich, and Centre for Environment, Fisheries and Aquaculture Science, Suffolk, United Kingdom

A. R. BAKER AND T. D. JICKELLS

Centre for Ocean and Atmospheric Sciences, School of Environmental Sciences, University of East Anglia, Norwich, United Kingdom

H. W. BANGE

GEOMAR Helmholtz Centre for Ocean Research Kiel, Kiel, Germany

R. J. CHANCE

Centre for Ocean and Atmospheric Sciences, School of Environmental Sciences, University of East Anglia, Norwich, and Wolfson Atmospheric Chemistry Laboratory, Department of Chemistry, University of York, York, United Kingdom

C. YODLE

Centre for Ocean and Atmospheric Sciences, School of Environmental Sciences, University of East Anglia, Norwich, United Kingdom

(Manuscript received 22 December 2014, in final form 16 June 2015)

ABSTRACT

Atmospheric deposition contributes potentially significant amounts of the nutrients iron, nitrogen, and phosphorus (via mineral dust and anthropogenic aerosols) to the oligotrophic tropical North Atlantic Ocean. Transport pathways, deposition processes, and source strengths contributing to this atmospheric flux are all highly variable in space and time. Atmospheric sampling was conducted during 28 research cruises through the eastern tropical North Atlantic (ETNA) over a 12-yr period, and a substantial dataset of measured concentrations of nutrients and trace metals in aerosol and rainfall over the region was acquired. This database was used to quantify (on a spatial and seasonal basis) the atmospheric input of ammonium, nitrate, soluble phosphorus, and soluble and total iron, aluminum, and manganese to the ETNA. The magnitude of atmospheric input varies strongly across the region, with high rainfall rates associated with the intertropical convergence zone contributing to high wet deposition fluxes in the south, particularly for soluble species. Dry deposition fluxes of species associated with mineral dust exhibited strong seasonality, with the highest fluxes associated with wintertime low-level transport of Saharan dust. Overall (wet plus dry) atmospheric inputs of soluble and total trace metals were used to estimate their soluble fractions. These also varied with season and were generally lower in the dry north than in the wet south. The ratio of ammonium plus nitrate to soluble iron in deposition to the ETNA was lower than the N:Fe requirement for algal growth in all cases, indicating the importance of the atmosphere as a source of excess iron.

Denotes Open Access content.

* Supplemental information related to this paper is available at the Journals Online website: http://dx.doi.org/10.1175/JAS-D-15-0011.s1.

Corresponding author address: A. R. Baker, School of Environmental Sciences, University of East Anglia, Earlham Road, Norwich NR4 7TJ, United Kingdom.
E-mail: alex.baker@uea.ac.uk

DOI: 10.1175/JAS-D-15-0011.1

1. Introduction

Atmospheric deposition accounts for approximately 70% of the input of iron (Fe) to the open ocean (Jickells et al. 2005) and is also an important source of fixed reactive nitrogen (N) (Duce et al. 2008; Krishnamurthy et al. 2007; Zamora et al. 2011) and soluble phosphorus (P) (Bristow et al. 2010; Mahowald et al. 2008; Ternon et al. 2011). This deposition has been shown to directly affect ocean biogeochemistry and primary production (Moore et al. 2009; Okin et al. 2011) with fundamentally different surface water biogeochemical regimes in the north and south tropical Atlantic as a result of dust deposition and its impact on the euphotic zone phytoplankton community. The eastern tropical North Atlantic (ETNA) is of interest because of its proximity to the Sahara Desert and Sahel region and also to the atmospheric transport pathway from North Africa and Europe, making it a region of particularly high atmospheric deposition. The flux of Saharan dust to the North Atlantic alone is estimated at 100–220 Tg yr^{-1} (Duce and Tindale 1991; Kaufman et al. 2005; Prospero et al. 1996) and is the predominant source of iron to the ETNA. In addition, a proportion of the nitrogen- and phosphorus-containing aerosols over the ETNA derive from the biomass burning products that are cotransported with Saharan dust (Chou et al. 2008; Crutzen and Andreae 1990; Real et al. 2010) and aerosols transported from Europe or northwest Africa (Savoie et al. 1989). However, the deposition of Saharan dust to and across this region varies on several different time scales from individual dust storms (on a time scale of days), through seasonality in dust production and transport, to interannual variability related at least in part to climate in dust source regions (Prospero et al. 2014). The nature of dust transport, and hence deposition, also varies seasonally. For example, maximum dust deposition to the Cape Verde Islands during the winter is associated with dust transport toward South America at lower levels in the atmosphere (Chiapello et al. 1995; Pye 1987), while peak Saharan dust transport to the Caribbean occurs during the summer months and is associated with transport above the marine boundary layer (Prospero and Lamb 2003; Prospero et al. 2012). This variability makes dust deposition, and therefore the atmospheric flux of nitrogen, phosphorus, and trace metals including iron to the ETNA, difficult to constrain.

Estimation of the atmospheric supply of nutrients to large oceanic areas, such as the ETNA, and prediction of future changes in this parameter generally requires the use of dust generation and atmospheric transport models (e.g., Luo et al. 2005; Mahowald et al. 2005). A great deal of information is required to validate these models. Satellite remote sensing can provide good measurements of aerosol mass transport and size distribution (Ben-Ami et al. 2009; Kaufman et al. 2005) but provides very little information on the chemical composition of the aerosol and deposition rates.

Records of aerosol and rainfall chemical composition have been obtained at several island sites, some over long time periods [e.g., Barbados (Prospero et al. 1996), Bermuda (Tian et al. 2008), and the Cape Verde Islands (Fomba et al. 2013; Fomba et al. 2014)]. However, the spatial coverage provided by such island sites is rather limited. Sampling from ships provides much better resolution over a larger spatial scale than island monitoring sites. However, shipboard sampling inevitably provides much poorer temporal resolution with relatively smaller numbers of samples than are possible at island sites, and this can make the use of ship data to derive deposition fluxes rather difficult.

Baker et al. (2010) and Baker et al. (2013) resolved this problem of representation by collating results obtained from aerosol and rainfall collection during multiple basin-scale cruises conducted over a 5-yr period to estimate climatological average atmospheric deposition of N, P, Fe, aluminum (Al), and manganese (Mn) to the whole Atlantic Ocean. They combined characteristic concentrations for aerosols originating from the major source regions around the basin with a climatology of airmass arrivals from those source regions to produce weighted average dry deposition fluxes to five broad areas of the Atlantic. For wet inputs, the available rainwater concentrations in each of those broad areas were pooled to produce volume-weighted mean concentrations, and these were used with climatological rainfall rates to estimate wet deposition. Baker et al. (2010) argued that seasonality in source emissions for N was likely to be low, and they therefore estimated annual average atmospheric inputs despite the nonuniform distribution of their sampling cruises through the year. However, Baker et al. (2013) recognized that this was unlikely to be the case for trace metals because mineral dust transport is strongly seasonal (e.g., Chiapello et al. 1995; Prospero and Lamb 2003; Pye 1987). They therefore restricted their estimates for Fe, Al, and Mn to the periods for which they had observations (April–June and September–November).

In this work, we use a unique database of aerosol and rain samples collected during 28 research cruises over a 12-yr period to estimate atmospheric inputs of N, P, and trace metals, including Fe, to the ETNA. This very large database allows us to quantify the seasonal and spatial distribution of wet and dry deposition to an ocean region with a biogeochemistry that is profoundly influenced by atmospheric deposition (Schlosser et al. 2014; Ussher et al. 2013).

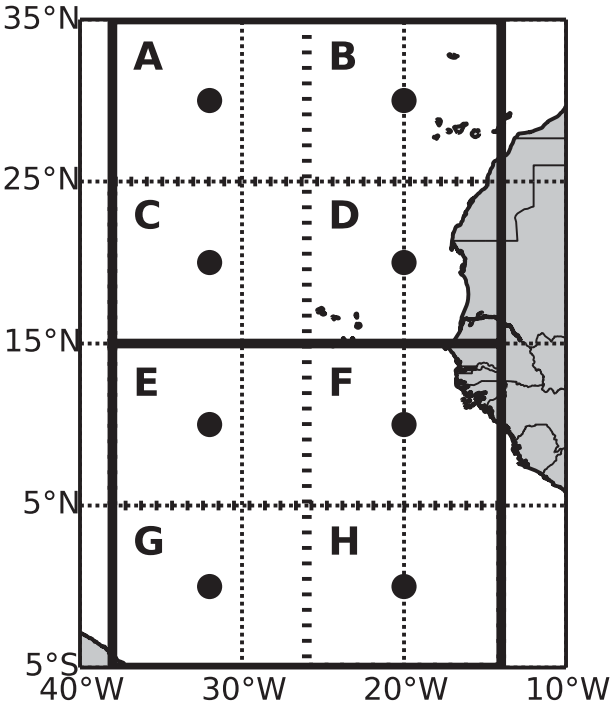

FIG. 1. Boundaries of the north and south regions of the ETNA (solid lines) and their subregions (A –H; dashed lines). Locations for which airmass back trajectories were obtained to define the air history for each subregion are shown with black dots.

2. Method

The procedures we have used to estimate atmospheric inputs to the ETNA are based on those we used in our earlier estimates of N and P (Baker et al. 2010) and trace metal (Baker et al. 2013) inputs to the wider Atlantic Ocean. Here, we consider the ETNA to be the area 5°S–35°N, 14°–38°W. The northern half of this region experiences very low rainfall rates, while rainfall rates in the southern half are much higher because of the influence of the intertropical convergence zone (ITCZ). The relative importance of wet deposition in the north and south of the ETNA is therefore expected to be rather different, and we make separate atmospheric input estimates for these two areas. As detailed below, we pool the available aerosol and rainwater concentration data for the periods March–May (MAM), June–August (JJA), September–November (SON) and December–February (DJF) into the north and south areas in order to assess seasonal variability. We further subdivide these areas each into four smaller boxes (see Fig. 1) and use these subregions to describe the variations in atmospheric transport pathways and dry and wet deposition rates on a finer spatial scale. We calculate atmospheric inputs for these subregions (see below) and sum these to produce the estimates for the north and south regions presented here.

Below we give an overview of the observational database used as the basis for our work and brief details of the sample collection and analysis methods used. Further details of sampling and analysis methods for individual cruises are given in the supplemental material and our previous publications.

a. Collection and analysis of samples

Between September 2000 and October 2011 we collected aerosol and rain samples during a total of 28 cruises in or through the ETNA region. Table 1 lists the dates and the number and type of samples collected within our study region for each cruise. Cruise tracks through the region with sampling locations for aerosol and rain samples are shown in Figs. 2 and 3, respectively. Further details of the cruises are given in Table S1 of the supplemental material for this article.

Aerosol samples were generally collected onto Whatman 41 (occasionally glass fiber) filters using high-volume aerosol samplers (flow rate: $1\,m^3\,min^{-1}$) for periods of around 24 h, with the ship facing into the wind to avoid contamination from the ship. Samples were either collected using Sierra-type cascade impactors, with separation into coarse- (aerodynamic particle diameter $> 1\,\mu m$) and fine-mode ($<1\,\mu m$) particles, or using a single bulk filter (see supplemental material; Baker et al. 2006, 2010, 2013, 2007). Aerosol samples were always stored at −20°C immediately after collection. For all 28 cruises, aerosol samples were analyzed for soluble major ions (MI), including nitrate (NO_3^-) and, in most cases, ammonium (NH_4^+). During 24 of the cruises, samples were collected for trace metal (TM) analysis. We report results for iron, aluminum, and manganese here. Soluble TMs were determined in all of these samples, and total TMs were determined for samples collected during 18 cruises. We also determined soluble phosphorus (SP) in the samples collected during 19 cruises. Total sample numbers were 348, 307, 304, 224, and 209 for NO_3^-, NH_4^+, soluble TMs, total TMs, and SP, respectively.

Rain samples were collected during 12 cruises using 28- or 40-cm-diameter polypropylene funnels attached to low-density polyethylene (LDPE) bottles. Two rain funnels were deployed simultaneously during each rain event: one for the collection of MI samples and the other for the collection of TM samples. The funnels were covered when not sampling to avoid contamination from the passive dry deposition of aerosols. Sampling and sample preservation methods are described by Baker et al. (2007). Total sample numbers were 45, 43, 8, and 41 for NO_3^-, NH_4^+, soluble TMs (samples filtered immediately after collection), and total TMs (unfiltered samples), respectively. Where precipitation samples were filtered, this was done immediately after collection. All precipitation samples

TABLE 1. Sample collection summary for the cruises used in this study. Samples are divided into two types: bulk (b; single filter) and size-segregated (ss) samples. All aerosol analytes include NO_3, NH_4, soluble TM (s-TM), total TM (t-TM), and SP. All rain (All-R) analytes include NO_3, NH_4, and total TM (t-TM).

		Aerosol samples			Rain samples	
Cruise	Dates within ETNA	No.	Type	Analytes	No.	Analytes
ANT18/1	Sep–Oct 2000	4	b, ss	NO_3, s- and t- TM, SP	1	NO_3, s- and t-TM
JCR	Sep–Oct 2001	8	ss	All	1	NO_3, NH_4
PEL	Oct 2002	12	b	NO_3, NH_4, s- and t-TM	—	—
M55	Oct–Nov 2002	20	ss	All	8	All-R, s-TM
AMT12	May–Jun 2003	12	ss	All	5	All-R
AMT13	Sep–Oct 2003	10	ss	All	5	All-R
24N	Apr–May 2004	10	b	NO_3, NH_4, SP	—	—
AMT14	Apr–Jun 2004	12	ss	All	5	All-R
FEEP	Apr–May 2004	8	b	All	—	—
AMT15	Sep–Oct 2004	11	ss	All	6	All-R
AIM	Mar–Apr 2005	11	b	All	—	—
AMT16	May–Jun 2005	5	b	All	—	—
AMT17	Oct–Nov 2005	11	ss	All	6	All-R
ANT23/1	Oct–Nov 2005	8	b	All	—	—
P332	Jan–Feb 2006	23	ss	All	1	NO_3, t-TM
M68/3	Jul–Aug 2006	20	ss	All	—	—
P348	Jan–Feb 2007	11	b	All	—	—
RMB	May 2007	14	ss	NO_3, NH_4	—	—
INSPIRE	Nov–Dec 2007	18	b	NO_3, NH_4	—	—
D326	Jan–Feb 2008	27	ss	All	1	NO_3, t-TM
ANT24/4	Apr–May 2008	9	b	NO_3, NH_4, SP	—	—
AMT18	Oct–Nov 2008	9	ss	NO_3, NH_4, s-TM, SP	—	—
ICON	Apr–May 2009	22	b	NO_3, s-TM	—	—
AMT19	Oct–Nov 2009	11	ss	NO_3, NH_4, s-TM	—	—
P399	Jun 2010	13	b	NO_3, s-TM	—	—
AMT20	Oct–Nov 2010	12	ss	NO_3, NH_4, s-TM	—	—
D361	Feb–Mar 2011	22	ss	NO_3, NH_4, s- and t-TM	5	All-R
AMT21	Oct 2011	13	ss	NO_3, NH_4, s-TM	2	NO_3, NH_4

were stored at −20°C prior to analysis. Precipitation samples for TM analysis were thawed and acidified to 15.8 mM Aristar HNO_3 at least 10 days before analysis. No SP analysis was performed on rain samples.

Sample analysis was generally by ion chromatography (NO_3^- and NH_4^+), inductively coupled plasma–optical emission spectrometry (ICP-OES; soluble TMs), instrumental neutron activation analysis (INAA; total TMs) and the molybdenum-blue spectrophotometric method (SP). For full details, see supplemental material and Baker et al. (2010, 2013).

b. *Dry deposition climatology*

As in our previous studies (Baker et al. 2010, 2013), we estimated atmospheric inputs via dry deposition by using our observations to characterize the chemical signature of the various source regions around the ETNA and by determining the frequency of occurrence of air originating from these source regions within each subregion of the ETNA.

The source region affecting individual aerosol samples was assigned based on 5-day airmass back trajectories from the NOAA HYSPLIT trajectory service (Draxler and Rolph 2003). We used the same source regions considered in our earlier studies (Baker et al. 2010, 2013). Those relevant for the ETNA were as follows: North American (NAM), remote North Atlantic (RNA), European (EUR), Saharan (SAH), Southern African (SAF), Southern African with a biomass burning signal (SAB), and remote Southern Atlantic (RSA). SAF and SAB air masses were distinguished on the basis of differences in their back trajectories at 1000 m (see Baker et al. 2006, 2010). Samples of the SAB type had non-sea-salt K^+ concentrations $> 1\,\text{nmol}\,\text{m}^{-3}$ (Baker et al. 2006). Air masses classified as RNA or RSA had not had contact with continental landmasses for 5 days prior to observation.

Representative concentrations for each source type were taken to be the median of all the observations of that source type in the north or south region for the season in question (see Table 2). Although we have a substantial observational database, we did not have enough data to define median concentrations for all source types in all regions and at all seasons. In such cases, we substituted values based on the available data

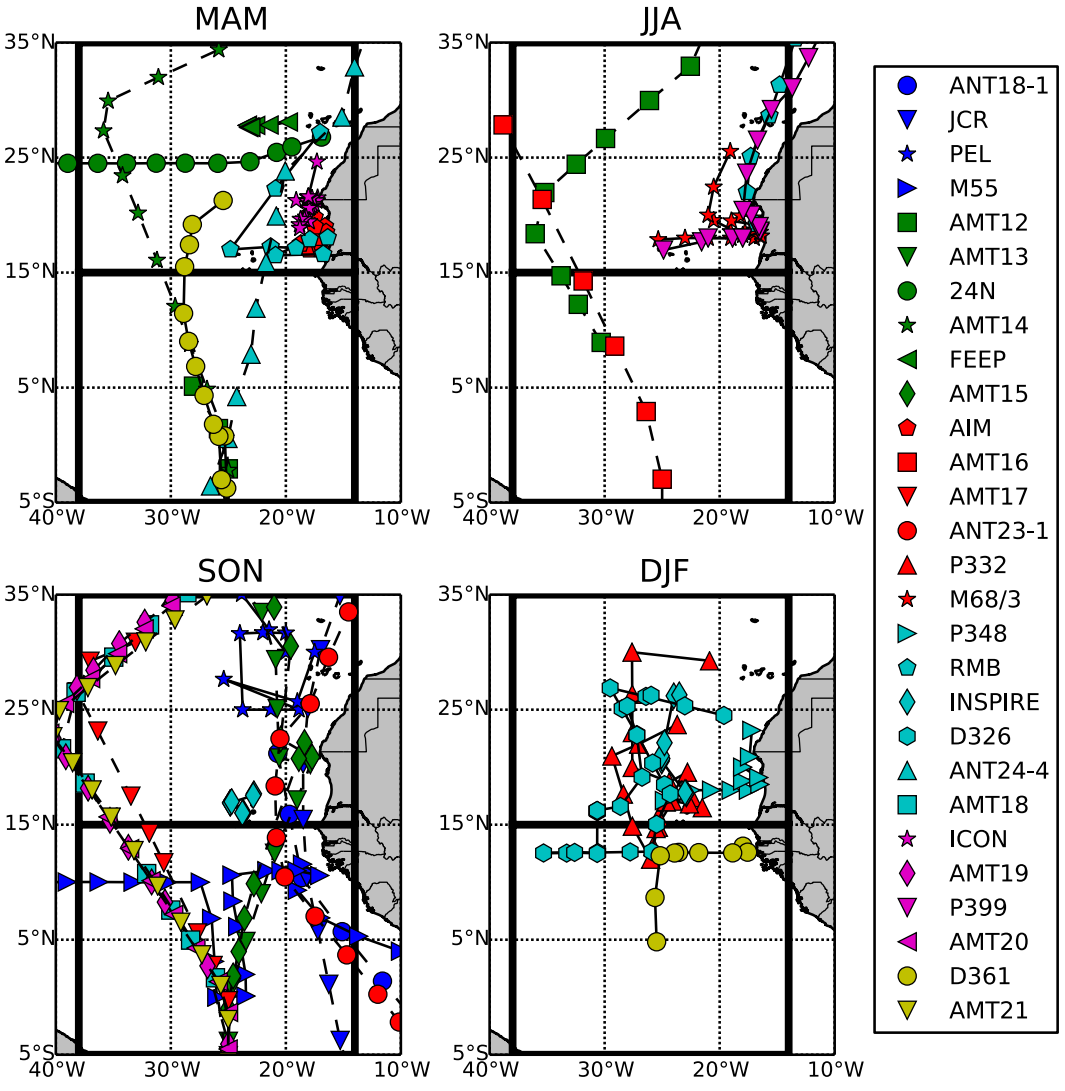

FIG. 2. Approximate cruise tracks and aerosol sample start locations used in this study, separated (top left to lower right) according to season. Symbol shapes are defined in the legend. Symbol colors indicate the time period of sample collections: 2000–02 (blue), 2003–04 (green), 2005–06 (red), 2007–08 (cyan), 2009–10 (magenta), and 2011–12 (yellow). Cruise tracks shown as solid lines occurred entirely within the ETNA; meridional transect cruises that passed through the region are shown as dashed lines. Only samples within the large black rectangle were included in this study.

for the same source type aerosols in adjacent regions or at other seasons. Details of these substitutions are also given in Table 2. Following Baker et al. (2010) and Baker et al. (2013), relative uncertainty values were assigned to these median concentrations based on the number of samples available to calculate each median. These relative uncertainties were as follows: 30% uncertainty for number of samples (n) between 5 and 10 and 15% for $n > 10$. In cases where we had 5 or fewer observations, we used substitute concentrations and assigned relative uncertainty values of 50% where we substituted concentrations for the same source type from a different region in the same season and 75% for all other substitutions.

Aerosol deposition fluxes were calculated from the median fine- and coarse-mode concentrations for each source type (i) using

$$F_d^i = \sum_i C_d^{i,m} v_d^m , \qquad (1)$$

where F_d^i is the dry deposition flux, $C_d^{i,m}$ is the atmospheric concentration of aerosol, $v_d^m$is the deposition velocity, and m refers to the fine- or coarse-size mode. As in our previous studies (Baker et al. 2010, 2013), we

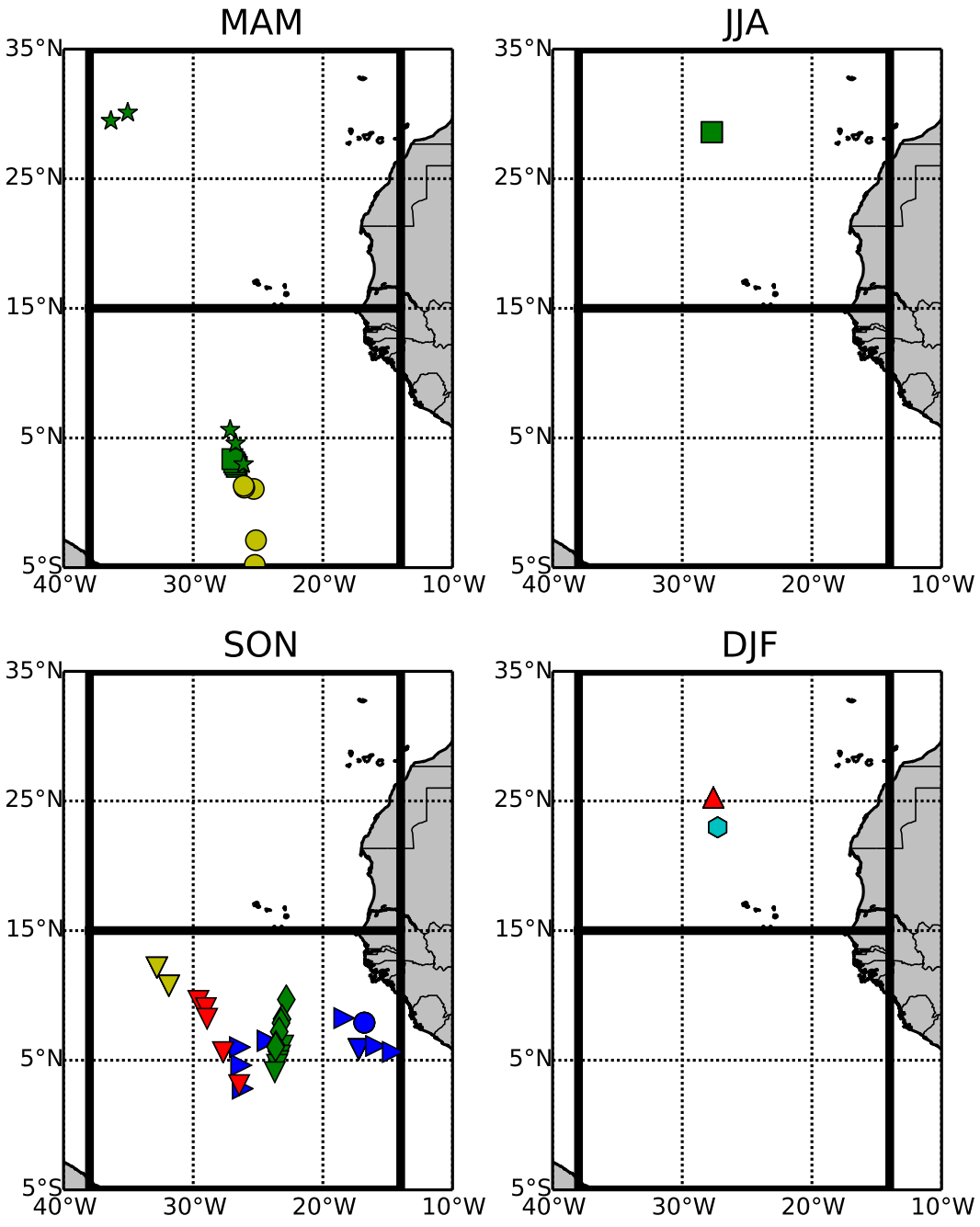

FIG. 3. Start locations of rain samples used in this study, separated according to (top left to lower right) season of collection. Symbol shapes and colors are as in Fig. 2.

artificially split concentration data for samples collected or analyzed as bulk aerosol into fine and coarse concentrations (see supplemental material). This was done using the same observations of median fine–coarse distributions used in those earlier works. Deposition velocities used were derived from the Ganzeveld et al. (1998) model, which depends on both particle mass median diameter (MMD) and wind speed. We used the same MMD values as used in our previous work (Baker et al. 2010, 2013): 0.6 μm for all fine-mode species, 5 μm for coarse-mode TMs, and 7 μm for coarse-mode N species and SP. The seasonally averaged wind speed for each subregion was determined using climatological wind speed data from the European Centre for Medium

TABLE 2. Median fine plus coarse aerosol concentrations (nmol m^{-3}) of NO_3^-, NH_4^+, SP, and soluble and total TMs in air from different origins collected in the north and south regions of the ETNA. Airmass origin codes are defined in the text. Corresponding fine- and coarse-mode concentrations can be found in Tables S4 and S5, respectively, and fine plus coarse concentration ranges and numbers of observations can be found in Table S6.

Season	Region	Air mass	Substitutions[a]	NH_4^+	NO_3^-	SP	s-Fe	s-Al	s-Mn	t-Fe	t-Al	t-Mn
MAM	North	NAM	S1									
		EUR	S2	31.5	48.7	0.029	0.076	0.29	0.017	1.56	4.17	0.034
		RNA		7.6	15.3	0.023	0.058	0.34	0.011	1.12	1.97	0.017
		SAH		16.6	32.5	0.070	0.220	1.50	0.085	9.26	34.0	0.160
	South	RNA	S3	1.1	2.5		0.012	0.24	0.016	0.76	2.12	0.019
		RSA	S4	4.3	4.2	0.014	0.035	0.23	0.011	1.46	4.22	0.027
		SAB	S5									
		SAF	S2	5.3	8.1	0.027	0.052	0.45	0.033	2.97	9.91	0.052
		SAH		14.7	19.5	0.058	0.095	0.71	0.055	5.54	20.4	0.111
JJA	North	NAM	S1									
		EUR	S2		33.8		0.052	0.22	0.009			
		RNA		16.1	15.0	0.037	0.078	0.59	0.020	3.09	11.9	0.060
		SAH		40.9	27.9	0.104	0.233	1.48	0.080	18.0	63.4	0.294
	South	RNA	S3	20.2	8.6	0.018	0.027	0.11	0.005	0.8	2.27	0.014
		RSA	S4									
		SAB	S5									
		SAF	S2	8.9	13.9	0.040	0.009	0.06	0.004	1.70	6.35	0.038
		SAH		0.8	20.6	0.019	0.078	0.72	0.064	11.8	42.3	0.206
SON	North	NAM	S1									
		EUR	S2	44.3	11.8		0.013	0.060	0.001			
		RNA		4.0	10.7	0.009	0.011	0.076	0.002	0.26	0.55	0.008
		SAH		13.0	20.4	0.059	0.168	1.61	0.117	11.5	37.5	0.17
	South	RNA	S3									
		RSA	S4									
		SAB		8.9	10.2	0.032	0.020	0.154	0.009	0.70	2.28	0.017
		SAF		10.8	8.8	0.025	0.033	0.176	0.009	0.83	1.90	0.017
		SAH		11.0	16.2	0.052	0.156	1.40	0.104	13.1	46.9	0.218
DJF	North	NAM	S1									
		EUR	S2	9.1	21.7	0.039	0.066	0.081	0.012	1.55	0.78	0.019
		RNA		6.2	7.5	0.029	0.026	0.133	0.007	0.44	0.88	0.010
		SAH		3.8	15.9	0.073	0.464	4.86	0.369	54.6	177	0.867
	South	RNA	S3	2.2	5.2	0.009	0.027	0.168	0.005	0.76	2.35	0.011
		RSA	S4									
		SAB	S5									
		SAF	S2									
		SAH		10.5	31.1	0.117	0.412	3.32	0.390	40.1	162	0.718

[a] Substitution types are as follows: used concentration for RNA type in same region, same season (S1); used median concentration of all values available for the type (S2); used concentration for RNA type in the north region, same season (S3); used concentration for RSA type from region 4 (southeast Atlantic) from Baker et al. (2010, 2013) (S4); used concentration for this type from SON (S5).

Range Weather Forecasting (ECMWF) Interim reanalysis dataset for data spanning 1999–2009 (ECMWF 2010). The resultant average wind speeds and dry deposition velocities are shown in Table 3.

The probability (w^i) of air from each source area occurring in each subregion of the ETNA was then used to calculate weighted average fluxes for each species using

$$F_d = \sum_0^z F_d^i w^i . \quad (2)$$

These probabilities were determined using 5-day airmass back trajectories for every 12 h between 14 March 1999 and 14 March 2009 using ECMWF archive data obtained from the British Atmospheric Data Centre (BADC). Each of these trajectories was assigned to a source type according to its location at 3 and 5 days, as described by Baker et al. (2010), and probabilities for each source type were calculated as the cumulative number of back trajectories assigned to that type, divided by the total number of trajectories. Source type probabilities for each subregion in each season can be found in Table 4. Uncertainties in median atmospheric concentration for each category were propagated using the same calculation in order to estimate uncertainty in the average aerosol deposition flux.

TABLE 3. Mean wind speed (u), dry deposition velocities (v_d) for particles with diameters of 0.6, 5, and 7 μm and mean precipitation rates (P) for each subregion in the seasons MAM, JJA, SON, and DJF.

Season	Subregion	u ($m\,s^{-1}$)	v_d ($m\,s^{-1}$) 0.6 μm	5 μm	7 μm	P ($m\,day^{-1}$)
MAM	A	6.8	0.0002	0.0063	0.0085	0.0012
	B	6.6	0.0002	0.0059	0.0081	0.0006
	C	7.4	0.0002	0.0076	0.0095	0.0003
	D	7.6	0.0002	0.0076	0.0095	0.0002
	E	7.7	0.0002	0.0080	0.0099	0.0010
	F	5.4	0.0002	0.0044	0.0067	0.0017
	G	5.2	0.0002	0.0042	0.0064	0.0078
	H	4.5	0.0002	0.0036	0.0055	0.0065
JJA	A	6.2	0.0002	0.0055	0.0077	0.0003
	B	6.6	0.0002	0.0059	0.0081	0.0002
	C	6.9	0.0002	0.0067	0.0088	0.0003
	D	8.1	0.0002	0.0084	0.0102	0.0005
	E	7.1	0.0002	0.0067	0.0088	0.0067
	F	4.7	0.0002	0.0038	0.0058	0.0081
	G	4.1	0.0002	0.0034	0.0050	0.0025
	H	4.1	0.0002	0.0034	0.0050	0.0013
SON	A	5.1	0.0002	0.0040	0.0061	0.0022
	B	6.6	0.0002	0.0059	0.0081	0.0011
	C	7.6	0.0002	0.0076	0.0095	0.0017
	D	7.4	0.0002	0.0076	0.0095	0.0008
	E	4.9	0.0002	0.0040	0.0061	0.0080
	F	4.4	0.0002	0.0036	0.0055	0.0064
	G	6.4	0.0002	0.0059	0.0081	0.0026
	H	5.8	0.0002	0.0047	0.0071	0.0018
DJF	A	5.7	0.0002	0.0047	0.0071	0.0020
	B	5.9	0.0002	0.0051	0.0074	0.0013
	C	6.5	0.0002	0.0059	0.0081	0.0010
	D	7.2	0.0002	0.0072	0.0092	0.0006
	E	5.3	0.0002	0.0042	0.0064	0.0024
	F	3.6	0.0002	0.0031	0.0046	0.0016
	G	6.8	0.0002	0.0063	0.0085	0.0060
	H	6.0	0.0002	0.0051	0.0074	0.0038

TABLE 4. Percentage occurrence (w^i) of air masses from the source regions affecting the ETNA for each subregion in the seasons MAM, JJA, SON, and DJF. Source region codes are defined in the text.

		Airmass source						
Season	Subregion	NAM	EUR	RNA	SAH	SAF	SAB	RSA
MAM	A	5.0	0.9	85.5	8.6			
	B	3.0	6.2	70.3	20.5			
	C	0.2	0.2	61.8	37.8			
	D	0.2	2.1	37.2	60.6			
	E			10.7				89.3
	F			3.9	0.1			96.0
	G			3.8	23.5	3.2	55.4	14.1
	H			0.2	21.5	13.0	64.3	0.9
JJA	A	0.2	0.1	93.1	6.6			
	B	0.4	1.1	84.3	14.2			
	C		0.3	40.3	59.4			
	D		0.9	25.4	73.7			
	E			30.8	29.0			40.2
	F			16.7	55.2			28.1
	G				21.2	12.0	66.6	0.2
	H				13.9	44.3	41.6	0.2
SON	A	2.1	1.7	82.3	13.9			
	B	1.2	7.5	70.1	21.2			
	C	0.2	1.0	36.5	62.3			
	D		1.6	14.2	84.2			
	E		0.1	28.9	19.0			52.1
	F			9.8	22.2			68.0
	G				10.3	24.0	65.2	0.5
	H			0.1	11.8	42.7	44.6	0.9
DJF	A	8.8	2.1	67.4	21.6			
	B	4.1	7.7	53.6	34.5			
	C	0.6	0.8	42.0	56.5			
	D	0.4	1.6	20.5	77.5			
	E			7.0	0.1			92.9
	F			0.9				99.1
	G			0.7	16.5		68.2	14.6
	H				20.9		76.9	2.2

c. *Wet deposition climatology*

We used data from the rain samples collected in the north or south regions to calculate volume-weighted mean (VWM) concentrations (C_V) for each species using

$$C_V = \frac{\sum_i (C_i V_i)}{\sum_i V_i} \tag{3}$$

where C_i are the individual sample concentrations, and V_i the individual collected sample volumes. Similarly to the approach used for our dry deposition estimate, we then combined these with precipitation rates for each subregion to estimate the wet deposition flux (see below). Rainfall rates in the north region are extremely low (Table 3), and we were only able to collect five rain samples there. We have calculated a VWM concentration for each species based on all these samples and used these concentrations to estimate wet deposition in each of the seasons. In the south region, we have more substantial sample numbers in MAM and SON and have calculated seasonal VWM concentrations for those periods. For JJA and DJF, we have used values of C_V calculated from all of the available rain samples in the south. Similar to our previous work (Baker et al. 2010), we assign relative uncertainties to these VWM concentrations based on the number of samples collected during each period. The values used for the south were 20% in SON ($n > 25$), 30% in MAM ($n > 10$), and 40% in JJA and DJF (for which we used substitute values; see Table 5). In the north, we assigned a relative uncertainty of 60% because of the low number of samples and the lack of effective seasonal information available.

TABLE 5. Volume-weighted mean rainfall concentrations (nmol L^{-1}) of NH_4^+, NO_3^-, and soluble and total TMs for samples collected in the north and south regions of the ETNA.

Region	Season	NH_4^+	NO_3^-	s-Fe	s-Al	s-Mn	t-Fe	t-Al	t-Mn	*n*
North	All	957	7590	26	186	25	394	1430	34	5
South	MAM	1690	6140	22	100	14	326	774	19	12
	JJA									0
	SON	5940	4510	21	133	16	492	1280	24	29
	DJF									0
	All	5220	4780	21	129	16	470	1210	23	41

As was the case for our earlier estimate for the Atlantic (Baker at al. 2013), although total TM concentrations were measured for all samples, there were very few rain samples for which soluble TM concentrations had been measured. As before, we used median soluble fraction values for Fe, Al, and Mn in Atlantic rainwater to calculate soluble trace metal concentrations for samples lacking a direct measurement of this parameter. The soluble fraction values used were 6.7%, 13%, and 74% for Fe, Al, and Mn, respectively. The value used for Fe was recalculated from that given by Baker et al. (2013) to include the data of Sedwick et al. (2007). Volume-weighted mean concentrations for each species are listed in Table 5.

The wet deposition flux was calculated from VWM concentration and the precipitation rate (Baker et al. 2010, 2013) using

$$F_W = C_V P, \tag{4}$$

where F_W is the wet flux and P is the precipitation rate. Precipitation rates for each subregion were calculated from monthly mean values obtained from the CPC Merged Analysis of Precipitation data (Xie and Arkin 1997) for the period August 1998 to July 2008. The values of P given in Table 3 demonstrate the low precipitation in the north of the ETNA and the migration of the ITCZ between ~15°N during July and ~5°S during January (Pye 1987).

3. Results and discussion

a. *Observational database: Aerosol signature concentrations of source regions*

As can be seen from Table 4, the majority of aerosol transported to each subregion is dominated by just one or two source types in any given season. Overall, the northern half of the ETNA is most strongly influenced by the RNA and SAH source regions, while, in the southern half, the relative importance of SAH, SAF, SAB, and RSA source types varies with season. The seasonal chemical signatures for source types for which we have the most complete seasonal record of observations are represented in Fig. 4, and a summary of median concentrations for all observed source types is provided in Table 2.

The concentrations of nitrate and ammonium do not vary significantly between seasons, aside from higher concentrations of NH_4^+ in the SAH and RNA airmass types during JJA in the northern half of the region. This broadly confirms the assumption made by Baker et al. (2010) that seasonality in nitrogen sources is low, at least for the ETNA. The majority of the other source types had too few samples to reliably assess their seasonality (see Table S4).

Buck et al. (2010) measured nitrate concentrations through the ETNA region in July/August 2003, finding median concentrations of 19.0, 25.3, and 21.6 nmol m^{-3} for North Atlantic maritime, Saharan, and tropical Atlantic maritime source regions respectively. These values are in good agreement with the median concentrations we report for the RNA, SAH, and SAF source types in JJA (Table 2). Johansen et al. (2000) measured concentrations of NO_3^- of less than 3.9–21.3 nmol m^{-3} and NH_4^+ concentrations of 3.8–16.6 nmol m^{-3} for a cruise across the tropical Atlantic during March and April, which also show good agreement with our results. The 5-year median aerosol concentrations for NO_3^- and NH_4^+ at the Cape Verde Atmospheric Observatory (CVAO) were 16.1 and 2.8 nmol m^{-3}, respectively (Fomba et al. 2014), which are both in relatively good agreement with the median concentrations for the northern half of the region. Fomba et al. (2014) reported maximum NH_4^+ concentrations at the CVAO during spring and early summer and suggested that this might result from a marine biogenic source. Interestingly, JJA NH_4^+ concentrations appear to be elevated in both the RNA and SAH source types in the north of the ETNA. The source of these higher NH_4^+ concentrations is unclear.

In contrast to the nitrogen species, the concentrations of soluble and total trace metals in the SAH source type in both the north and south are particularly high during DJF. Similar patterns were observed for SP. These results are in line with observations by Chiapello et al. (1995) and Fomba et al. (2013), who reported maximum dust concentrations at the Cape Verde Islands during

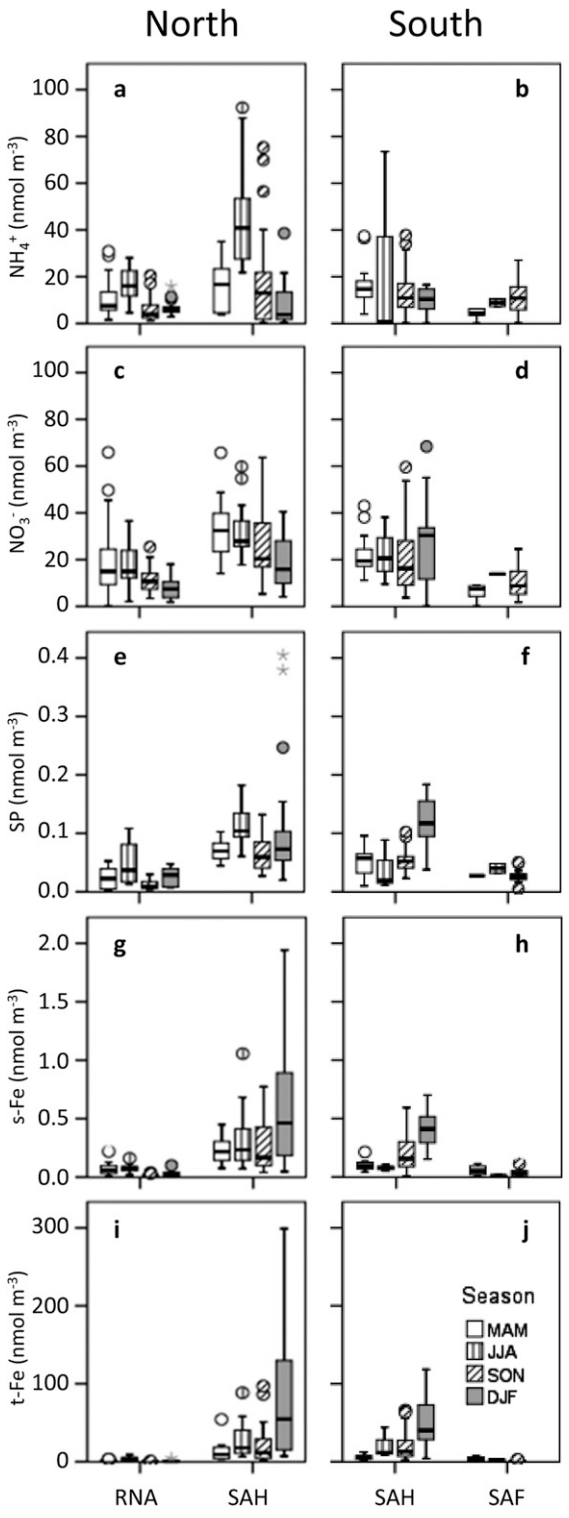

FIG. 4. Box-and-whisker plots showing the seasonal variation in the aerosol concentrations in selected airmass types for (left) north and (right) south of the ETNA: (a),(b) NH_4^+; (c),(d) NO_3^-; (e),(f) SP; (g),(h) s-Fe; and (i),(j) t-Fe . Boxes show interquartile range and whiskers show range, except where outliers (>1.5 × the interquartile range: circles) or extremes (>3 × the interquartile range: stars) are present.

winter. Strong winter deposition of dust from trade winds has also been observed in sediments from the eastern equatorial Atlantic (Stuut et al. 2005). In JJA, high-level transport in the Saharan air layer carries large amounts of dust across the Atlantic to the Caribbean and North America (Prospero et al. 2014). However, our results suggest that little of this material is found at the surface of the ETNA covered by our study. The relatively low concentrations of TMs we observed (with respect to those observed in DJF) are consistent with satellite-borne lidar observations, which show that most dust transported over our study region in JJA occurs above the marine boundary layer (Adams et al. 2012).

Fomba et al. (2013) report mean aerosol concentrations of 0.11 and 0.002 nmol m^{-3} for total Fe and Mn in air with origins over the remote North Atlantic. Additionally, the aerosol samples collected by Buck et al. (2010) over the ETNA had median July–August concentrations for North Atlantic maritime origin air of 0.077, <0.25, and 0.008 nmol m^{-3} for total Fe, Al, and Mn, respectively; 4.35, 11.2, and 0.080 nmol m^{-3} for the Saharan source region type; and 0.339, 0.823, and 0.016 nmol m^{-3} for tropical Atlantic maritime airmass types. These all lie broadly within the range of concentrations presented in Table S4.

b. *Observational database: Volume-weighted mean rain concentrations*

Table 5 shows the volume-weighted mean rainfall concentrations used to calculate the wet deposition fluxes. Concentrations of most species were slightly higher in the north than in the south, although with so few samples available for the north it is not clear whether this difference is representative.

There are not many published rainwater concentrations for nutrients or trace metals for this area, but Buck et al. (2010) report rainwater concentrations during June and July within the southern half of the ETNA of 18.2–159 nmol L^{-1} for s-Fe, 132–419 nmol L^{-1} for t-Fe, 74.4–523 nmol L^{-1} for s-Al, and 413–1400 nmol L^{-1} for t-Al, which is in broad agreement with the values in Table 5. Kim and Church (2002) also report rainwater Fe concentrations of 590–2150 nmol L^{-1} and Mn concentrations of 25–130 nmol L^{-1} for the south of the ETNA in June 1996. Helmers and Schrems (1995) reported Fe, Al, and Mn concentrations of 150–1140, 330–4860, and 8.3–62 nmol L^{-1}, respectively, in rainfall from the ITCZ in October 1990.

c. *Climatology: Wet and dry deposition fluxes to the ETNA*

The seasonal atmospheric deposition fluxes of NH_4^+, NO_3^-, soluble Fe, and total Fe for the ETNA are shown in Fig. 5. Flux rates for all species are summarized in

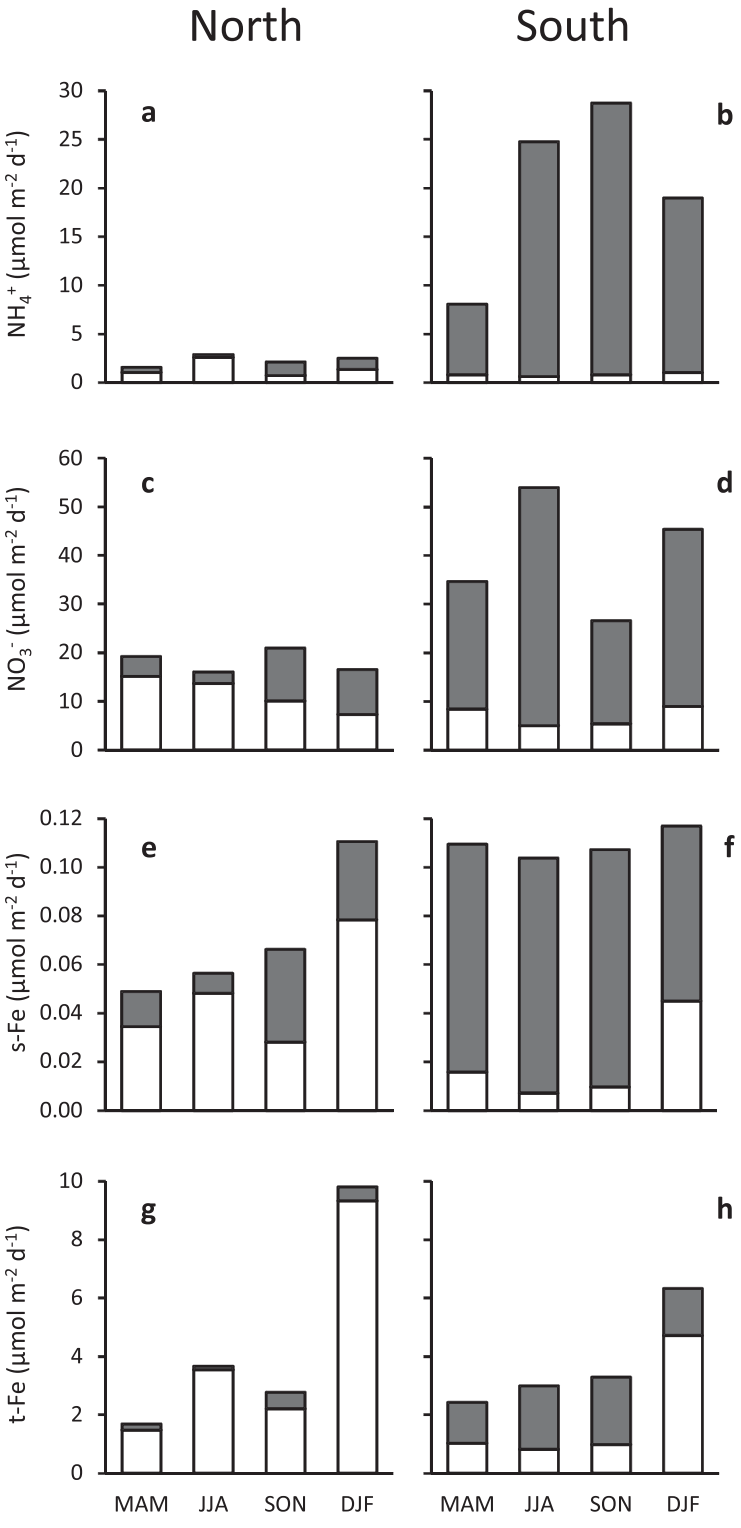

FIG. 5. Dry (white) and wet (gray) seasonal deposition fluxes for (left) north and (right) south of the ETNA of (a),(b) NH_4^+; (c),(d) NO_3^-; (e),(f) s-Fe; and (g),(h) t-Fe.

TABLE 6. Dry (D), wet (W), and total (D + W; italic) deposition fluxes (μmol m^{-2} d^{-1}) of NO_3^-, NH_4^+, SP, and soluble and total TMs to the north and south regions of the ETNA.

Season	Region	Mode	NH_4^+	NO_3^-	SP	s-Fe	s-Al	s-Mn	t-Fe	t-Al	t-Mn
MAM	North	D	1.1	15.1	0.014	0.034	0.24	0.016	1.5	5.1	0.03
		W	0.5	4.1		0.014	0.10	0.013	0.2	0.8	0.02
		D+W	*1.6*	*19.2*		*0.049*	*0.34*	*0.029*	*1.7*	*5.9*	*0.04*
	South	D	0.8	8.4	0.011	0.016	0.12	0.012	1.0	3.8	0.02
		W	7.2	26.3		0.094	0.43	0.061	1.4	3.3	0.08
		D+W	*8.1*	*34.7*		*0.110*	*0.55*	*0.073*	*2.4*	*7.1*	*0.10*
JJA	North	D	2.6	13.7	0.021	0.048	0.37	0.023	3.5	13.2	0.06
		W	0.3	2.4		0.008	0.06	0.008	0.1	0.4	0.01
		D+W	*2.9*	*16.1*		*0.056*	*0.43*	*0.030*	*3.7*	*13.6*	*0.07*
	South	D	0.6	5.0	0.006	0.007	0.06	0.005	0.8	3.0	0.02
		W	24.1	48.9		0.097	0.60	0.073	2.2	5.6	0.11
		D+W	*24.8*	*54.0*		*0.104*	*0.66*	*0.078*	*3.0*	*8.6*	*0.12*
SON	North	D	0.8	10.1	0.011	0.028	0.22	0.025	2.2	7.4	0.03
		W	1.4	10.9		0.038	0.27	0.036	0.6	2.1	0.05
		D+W	*2.1*	*21.0*		*0.066*	*0.49*	*0.060*	*2.8*	*9.4*	*0.08*
	South	D	0.8	5.4	0.009	0.010	0.09	0.009	1.0	3.5	0.02
		W	27.9	21.2		0.098	0.63	0.075	2.3	6.0	0.11
		D+W	*28.7*	*26.6*		*0.107*	*0.71*	*0.084*	*3.3*	*9.5*	*0.13*
DJF	North	D	1.4	7.3	0.016	0.078	0.77	0.065	9.3	31.1	0.16
		W	1.2	9.2		0.032	0.23	0.030	0.5	1.7	0.04
		D+W	*2.5*	*16.6*		*0.111*	*1.00*	*0.096*	*9.8*	*32.8*	*0.20*
	South	D	1.0	9.0	0.024	0.045	0.36	0.048	4.7	19.3	0.09
		W	17.9	36.4		0.072	0.44	0.054	1.6	4.2	0.08
		D+W	*19.0*	*45.4*		*0.117*	*0.81*	*0.102*	*6.3*	*23.4*	*0.17*

Table 6, with total atmospheric inputs for each season given in Table 7. The differing precipitation rates in the north and south of the ETNA appear to have a major impact on the mode, magnitude, and seasonality of the atmospheric deposition of nutrients and trace metals.

Wet deposition is the dominant mode (>80% of total) for most species in the south, and dry deposition rates are lower there than in the north. Higher precipitation rates, lower dry deposition velocities (caused by lower wind speeds), and slightly lower aerosol concentrations in the south may all contribute to this. In the north, the wet deposition contributes 15%–50% of the total NO_3^- flux, with the highest dry–wet ratio being observed during JJA. Similar dry–wet ratios were observed for ammonium. In contrast, in the south, the wet flux of NO_3^- was 76%–91% of the total, with corresponding values of 90%–97% for NH_4^+. The importance of wet deposition is much lower for total Fe and Al. In contrast, wet deposition makes a larger contribution to the flux of total Mn in the south (>75% in most seasons). This effect results in the preferential removal of total Mn in wet deposition (as compared to total Al and Fe), and this implies that at least a fraction of Mn is not internally mixed with Fe and Al in dust aerosol. We have previously noted similar behavior for the Atlantic as a whole and suggested that the effect is probably related to the higher solubility of Mn (Baker et al. 2013).

For most species, atmospheric fluxes are higher to the south throughout the year, again because of the influence of wet deposition there. There is very little seasonality in deposition fluxes of N species to the north but more variability in wet fluxes to the south (Fig. 5). To some extent, the variations in NH_4^+ and NO_3^- oppose one another (e.g., in SON), but the total inorganic N flux to the south in MAM is ~56% of the equivalent flux in SON. The dry deposition fluxes of the dust-associated species (SP, Fe, Al, and Mn) all show strong seasonality, primarily driven by low-level dust transport in DJF (Chiapello et al. 1995). In the north, these species also exhibit relatively high fluxes in JJA, probably as a result of dust deposited from the high-level Saharan air layer transport (Prospero et al. 2014).

Assuming dust contains 8% by mass Al, our results indicate that the north and south of the ETNA receive on average ~10.1 and 8.8 Tg dust yr^{-1}, respectively.

In Table 8, we illustrate the effect that uncertainty in characteristic aerosol concentrations and rainwater VWM concentrations (see sections 2b and 2c) introduces into our calculations. Although we assigned relative uncertainties in our dry deposition calculation of up to 75% for poorly sampled aerosol source types, the overall uncertainty in the dry deposition flux (or input) calculations was below 20% in most cases. This indicates that the climatologically most important aerosol source

TABLE 7. Dry (D), wet (W), and total (D+W; italic) atmospheric input (Gmol region^{-1} season^{-1}) of NO_3^-, NH_4^+, SP, and soluble and total TMs to the north and south regions of the ETNA for the seasons MAM, JJA, SON, and DJF.

Season	Region	Mode	NH_4^+	NO_3^-	SP	s-Fe	s-Al	s-Mn	t-Fe	t-Al	t-Mn
MAM	North	D	0.5	7.5	0.007	0.017	0.12	0.008	0.7	2.5	0.01
		W	0.3	2.0		0.007	0.05	0.007	0.1	0.4	0.01
		D+W	*0.8*	*9.5*		*0.024*	*0.17*	*0.014*	*0.8*	*2.9*	*0.02*
	South	D	0.4	4.6	0.006	0.009	0.06	0.006	0.6	2.0	0.01
		W	3.9	14.3		0.051	0.23	0.033	0.8	1.8	0.04
		D+W	*4.4*	*18.8*		*0.059*	*0.30*	*0.040*	*1.3*	*3.8*	*0.06*
JJA	North	D	1.3	6.8	0.011	0.024	0.18	0.011	1.7	6.5	0.03
		W	0.1	1.2		0.004	0.03	0.004	0.1	0.2	0.01
		D+W	*1.4*	*7.9*		*0.028*	*0.21*	*0.015*	*1.8*	*6.7*	*0.04*
	South	D	0.3	2.7	0.003	0.004	0.03	0.003	0.4	1.6	0.01
		W	13.1	26.5		0.052	0.32	0.040	1.2	3.0	0.06
		D+W	*13.4*	*29.3*		*0.056*	*0.36*	*0.042*	*1.6*	*4.6*	*0.07*
SON	North	D	0.4	4.9	0.006	0.014	0.11	0.012	1.1	3.6	0.02
		W	0.7	5.3		0.019	0.13	0.017	0.3	1.0	0.02
		D+W	*1.0*	*10.2*		*0.032*	*0.24*	*0.030*	*1.4*	*4.6*	*0.04*
	South	D	0.4	2.9	0.005	0.005	0.05	0.005	0.5	1.9	0.01
		W	15.0	11.4		0.052	0.34	0.040	1.2	3.2	0.06
		D+W	*15.4*	*14.3*		*0.058*	*0.38*	*0.045*	*1.8*	*5.1*	*0.07*
DJF	North	D	0.7	3.5	0.008	0.038	0.37	0.032	4.5	15.0	0.08
		W	0.6	4.5		0.016	0.11	0.015	0.2	0.8	0.02
		D+W	*1.2*	*8.0*		*0.053*	*0.48*	*0.046*	*4.7*	*15.9*	*0.10*
	South	D	0.5	4.8	0.013	0.024	0.19	0.025	2.5	10.2	0.05
		W	9.5	19.3		0.038	0.24	0.029	0.9	2.2	0.04
		D+W	*10.1*	*24.1*		*0.062*	*0.43*	*0.054*	*3.4*	*12.4*	*0.09*

types (see Table 4) are well represented in our observational database in most cases. Notable exceptions to this occur in the south in JJA, where we have relatively few observations for any of the species (Fig. 2). Similarly, the high relative uncertainty (60%) we assigned to the rainwater VWM concentrations in the north had relatively little impact on the overall (dry plus wet) uncertainty in that region because of the low precipitation rates there. Overall, uncertainties using these approaches were in the range 14% (t-Al in the south in SON) to 40% (NH_4^+ in the north in SON).

We have also examined the influence of variability in source-type aerosol concentrations on the magnitude of our dry deposition estimates. To do so, we repeated our dry flux calculations using lower- and upper-quartile aerosol concentrations for each species and source type, instead of the median values used in our baseline calculations. In Table S7, we compare, on a regional and seasonal basis, the results of these calculations to our baseline estimates (Table 6) and the dry flux uncertainty calculated on the basis of numbers of samples collected (Table 8). We also represent the uncertainty in dry inputs to the whole ETNA using both methods in Fig. S1. For some species, notably NO_3^- and SP, the two uncertainty estimates are similar, but for the trace metals, and in particular the total trace metals, the uncertainty estimated using the interquartile range is higher by at least a factor of two (Table S7). As indicated above, the impact of these higher dry uncertainties will be greater in the north than in the south.

In addition to the factors discussed above, there are a number of sources of uncertainty in our estimates of dry and wet deposition to the ETNA. For dry deposition, these include the following: the representativeness of the aerosol samples collected (in terms of their expected frequency of occurrence for a given air source type and their spatial distribution within the ETNA), dry deposition velocities, and the effects of our choices of mean particle diameters and fractions of total aerosol concentrations in the coarse and fine mode (where these were not directly measured) on calculated dry deposition fluxes. For wet deposition, sources of uncertainty include the spatial distribution and numbers of rain samples, as well as the estimates of precipitation rates used to calculate wet deposition fluxes. We have discussed these factors in detail in our earlier studies (Baker et al. 2010, 2013) and direct the interested reader to those works.

Of those factors, we consider uncertainty in the absolute accuracy of estimated dry deposition velocities and poor characterization of rainfall composition as a result of limited sampling (particularly in the north) to dominate the uncertainty in dry and wet deposition estimates, respectively. Duce et al. (1991) estimated that the uncertainty in dry deposition velocities was

TABLE 8. Relative uncertainties (%) arising from uncertainties in representative concentrations used to characterize dry, wet, and total (italic) atmospheric deposition flux/input of NO_3^-, NH_4^+, SP, and soluble and total TMs to the north and south regions of the ETNA for the seasons MAM, JJA, SON, and DJF.

Season	Region	Mode	NH_4^+	NO_3^-	SP	s-Fe	s-Al	s-Mn	t-Fe	t-Al	t-Mn
MAM	North	D	22	18	26	16	16	16	28	29	29
		W	60	60		60	60	60	60	60	60
		D+W	*24*	*19*		*21*	*21*	*29*	*26*	*26*	*30*
	South	D	42	28	43	35	36	34	34	32	33
		W	30	30		30	30	30	30	30	30
		D+W	*27*	*24*		*26*	*25*	*26*	*22*	*22*	*25*
JJA	North	D	16	16	15	15	15	15	17	18	18
		W	60	60		60	60	60	60	60	60
		D+W	*15*	*16*		*16*	*15*	*19*	*17*	*17*	*17*
	South	D	71	79	91	40	40	45	62	66	67
		W	40	40		40	40	40	40	40	40
		D+W	*39*	*37*		*37*	*37*	*37*	*34*	*35*	*36*
SON	North	D	25	18	16	16	15	15	15	15	16
		W	60	60		60	60	60	60	60	60
		D+W	*40*	*32*		*35*	*33*	*36*	*17*	*18*	*35*
	South	D	22	20	22	17	16	16	16	16	17
		W	20	20		20	20	20	20	20	20
		D+W	*19*	*16*		*18*	*18*	*18*	*15*	*14*	*17*
DJF	North	D	23	20	20	15	15	15	15	15	15
		W	60	60		60	60	60	60	60	60
		D+W	*30*	*35*		*21*	*18*	*22*	*15*	*15*	*17*
	South	D	43	30	38	18	18	17	17	16	17
		W	40	40		40	40	40	40	40	40
		D+W	*38*	*33*		*26*	*23*	*23*	*16*	*15*	*21*

approximately a factor of 2–3. The significance of this uncertainty varies markedly across the ETNA. For example, in the north in JJA, doubling the dry deposition velocity increases the overall atmospheric input by 73%–97%, depending on species, whereas the same increase in the south would increase the overall atmospheric input by only 2%–35% in the same season.

d. Trace metal soluble fraction

Overall percentage soluble fractions [(100 × dry plus wet input of soluble TM) ÷ (dry plus wet input of total TM)] for Fe, Al, and Mn are shown in Table 9. As we have noted previously (Baker et al. 2013), these values take account of the input of material from multiple sources, via both dry and wet deposition, and over time periods comparable to the residence times of TMs in surface seawater (Croot et al. 2004). They therefore more accurately represent the environmental behavior of atmospheric inputs to the ETNA than measurements made on individual aerosol or rainwater samples.

Soluble fractions were generally higher in the south, driven by the higher TM solubility in rainwater than aerosol and the high rainfall rate there. In both the north and south, the lowest soluble fractions for all the TMs were observed in DJF when (lower solubility) dry dust deposition was at its highest. For all the TMs, there appears to be a weak relationship between overall soluble fraction and the percentage of total TM in wet deposition [(100 × wet input) ÷ (dry + wet input)]; relationship not shown]. For Fe, soluble fraction varies from 1%–1.5% at ~5% wet deposition of total Fe to 3%–4% at ~70% wet deposition.

e. Nitrogen to iron ratios

Our concurrent estimates of NH_4^+, NO_3^-, and soluble Fe inputs to the ETNA allow us to determine the (inorganic) N:s-Fe ratio of atmospheric deposition to the region (Fig. 6). Further atmospheric input of N to the ETNA will occur as a result of deposition of other species, such as aerosol and rainwater organic N (e.g., Lesworth et al. 2010) and gas phase NH_3 and HNO_3, so

TABLE 9. Overall soluble fractions (%) of Fe, Al, and Mn in atmospheric deposition to the north and south regions of the ETNA for the seasons MAM, JJA, SON, and DJF.

Season	Region	Fe	Al	Mn
MAM	North	2.9	5.7	65.3
	South	4.5	7.7	69.6
JJA	North	1.5	3.2	41.5
	South	3.5	7.7	63.3
SON	North	2.4	5.2	72.6
	South	3.3	7.5	64.5
DJF	North	1.1	3.0	48.0
	South	1.8	3.4	60.0

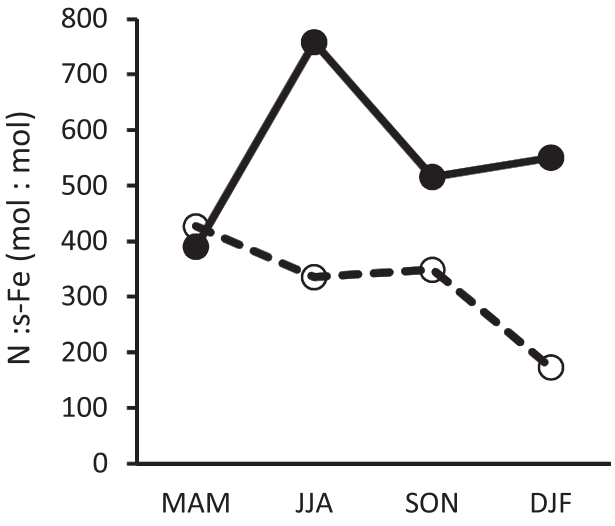

FIG. 6. Variation with season of the overall (wet + dry) atmospheric deposition ratio of N (NH_4^+ + NO_3^-) to s-Fe in the north (open) and south (solid) of the ETNA.

the N:s-Fe ratios we quote are lower limits. For most of the year, this ratio is higher in the south than the north because of the high rates of wet N deposition in the south. In the north, N:s-Fe is extremely low in the DJF dusty period. We compare these values to the N:Fe quota for algal growth under Fe-replete conditions (11 600 mol mol^{-1}; Sunda 1997) and note that the atmospheric input to the ETNA is considerably enriched in Fe, relative to these requirements, throughout the year. While algal productivity in much of the ETNA is likely to be limited by N availability, atmospheric deposition has the potential to supply external Fe to meet the requirements of nitrogen-fixing primary producers there (Mills et al. 2004). Note, however, that in waters that receive abundant supplies of mineral dust, such as the ETNA, dissolution of Fe from atmospheric deposition is likely to be controlled by the Fe saturation state of the receiving seawater (Baker and Croot 2010). This effect is likely to reduce the extent of Fe dissolution upon deposition to the ETNA and therefore lead to higher N:s-Fe ratios for the atmospheric input than calculated here.

4. Conclusions

Using results obtained from the analysis of ~350 aerosol and ~45 rain samples collected during 28 research cruises, we have estimated the average atmospheric inputs of NH_4^+, NO_3^-, SP, and the trace metals Fe, Al, and Mn to the ETNA. Total inputs of the nutrients NH_4^+, NO_3^-, SP, and soluble Fe to the ETNA were 48, 122, 0.058, and 0.37 Gmol yr^{-1}, respectively (with the SP estimate being for dry deposition only). Note that our estimates for NH_4^+ do not directly include the influence of air–sea gas exchange of NH_3 (Johnson et al. 2008). Our study reveals the spatial and seasonal variations in atmospheric deposition to the ETNA and highlights the significant roles played by the distribution of, and variations in, rainfall (particularly in the ITCZ) and the source strength and altitude of atmospheric transport of mineral dust generated in the Sahara/Sahel region. This dynamic atmospheric deposition regime has a major impact on the biogeochemistry of the ETNA (Schlosser et al. 2014).

Our deposition estimates allow us to calculate overall soluble fractions for the trace metals and the N:s-Fe ratio of the atmospheric input. The former appear to increase with the percentage of TM deposited by wet deposition, while the latter implies a large excess (relative to algal requirements) of atmospheric Fe supply to the ETNA.

Acknowledgments. We thank the colleagues named in Table S1 who contributed to sample collection during many cruises through the ETNA. This study was supported by the U.K. Natural Environment Research Council (NERC) through Grants NE/C001737/1, NE/E010180/1, NE/G016585/1, and NE/F017359/1 and by the German SOPRAN project (www.sopran.pangaea.de) through Grants FKZ03F0462A and FKZ03F0611A. Atlantic Meridional Transect (AMT) cruises 18–21 were supported by the U.K. NERC National Capability funding to Plymouth Marine Laboratory and the National Oceanography Centre, Southampton. This is contribution 271 of the AMT program. We gratefully acknowledge the NOAA Air Resources Laboratory for the provision of the HYSPLIT transport and dispersion model and READY website (http://www.arl.noaa.gov/ready.html) used in this publication. ECMWF ERA-Interim data used in this study have been obtained from the ECMWF data server. The rainwater and aerosol chemical data used in this study are available from the COST735 marine aerosol and rain chemistry database (http://www.bodc.ac.uk/solas_integration/implementation_products/group1/aerosol_rain/). We appreciate the helpful comments of three anonymous reviewers.

REFERENCES

Adams, A., J. Prospero, and C. Zhang, 2012: *CALIPSO*-derived three-dimensional structure of aerosol over the Atlantic basin and adjacent continents. *J. Climate*, **25**, 6862–6879, doi:10.1175/JCLI-D-11-00672.1.

Baker, A. R., and P. L. Croot, 2010: Atmospheric and marine controls on aerosol iron solubility in seawater. *Mar. Chem.*, **120**, 4–13, doi:10.1016/j.marchem.2008.09.003.

——, T. D. Jickells, K. F. Biswas, K. Weston, and M. French, 2006: Nutrients in atmospheric aerosol particles along the Atlantic Meridional Transect. *Deep-Sea Res. II*, **53**, 1706–1719, doi:10.1016/j.dsr2.2006.05.012.

——, K. Weston, S. D. Kelly, M. Voss, P. Streu, and J. N. Cape, 2007: Dry and wet deposition of nutrients from the tropical Atlantic atmosphere: Links to primary productivity and nitrogen fixation. *Deep-Sea Res. I*, **54**, 1704–1720, doi:10.1016/j.dsr.2007.07.001.

——, T. Lesworth, C. Adams, T. D. Jickells, and L. Ganzeveld, 2010: Estimation of atmospheric nutrient inputs to the Atlantic Ocean from 50°N to 50°S based on large-scale field sampling: Fixed nitrogen and dry deposition of phosphorus. *Global Biogeochem. Cycles*, **24**, GB3006, doi:10.1029/2009GB003634.

——, C. Adams, T. G. Bell, T. D. Jickells, and L. Ganzeveld, 2013: Estimation of atmospheric nutrient inputs to the Atlantic Ocean from 50°N to 50°S based on large-scale field sampling: Iron and other dust-associated elements. *Global Biogeochem. Cycles*, **27**, 755–767, doi:10.1002/gbc.20062.

Ben-Ami, Y., I. Koren, and O. Altaratz, 2009: Patterns of North African dust transport over the Atlantic: Winter vs. summer, based on CALIPSO first year data. *Atmos. Chem. Phys.*, **9**, 7867–7875, doi:10.5194/acp-9-7867-2009.

Bristow, C. S., K. A. Hudson-Edwards, and A. Chappell, 2010: Fertilizing the Amazon and equatorial Atlantic with West African dust. *Geophys. Res. Lett.*, **37**, L14807, doi:10.1029/2010GL043486.

Buck, C. S., W. M. Landing, J. A. Resing, and C. I. Measures, 2010: The solubility and deposition of aerosol Fe and other trace elements in the North Atlantic Ocean: Observations from the A16N CLIVAR/CO_2 repeat hydrography section. *Mar. Chem.*, **120**, 57–70, doi:10.1016/j.marchem.2008.08.003.

Chiapello, I., G. Bergametti, L. Gomes, B. Chatenet, F. Dulac, J. Pimenta, and E. S. Suares, 1995: An additional low layer transport of Sahelian and Saharan dust over the north-eastern tropical Atlantic. *Geophys. Res. Lett.*, **22**, 3191–3194, doi:10.1029/95GL03313.

Chou, C., P. Formenti, M. Maille, P. Ausset, G. Helas, M. Harrison, and S. Osbourne, 2008: Size distribution, shape, and composition of mineral dust aerosols collected during the African Monsoon Multidisciplinary Analysis Special Observation Period 0: Dust and Biomass-Burning Experiment field campaign in Niger, January 2006. *J. Geophys. Res.*, **113**, D00C10, doi:10.1029/2008JD009897.

Croot, P. L., P. Streu, and A. R. Baker, 2004: Short residence time for iron in surface seawater impacted by atmospheric dry deposition from Saharan dust events. *Geophys. Res. Lett.*, **31**, L23S08, doi:10.1029/2004GL020153.

Crutzen, P. J., and M. O. Andreae, 1990: Biomass burning in the tropics: Impact on atmospheric chemistry and biogeochemical cycles. *Science*, **250**, 1669–1678, doi:10.1126/science.250.4988.1669.

Draxler, R. R., and G. D. Rolph, 2003: HYSPLIT—Hybrid Single Particle Lagrangian Integrated Trajectory Model. NOAA/Air Resources Laboratory. [Available online at http://www.arl.noaa.gov/ready/hysplit4.html.]

Duce, R. A., and N. W. Tindale, 1991: Atmospheric transport of iron and its deposition in the ocean. *Limnol. Oceanogr.*, **36**, 1715–1726, doi:10.4319/lo.1991.36.8.1715.

——, and Coauthors, 1991: The atmospheric input of trace species to the world ocean. *Global Biogeochem. Cycles*, **5**, 193–259, doi:10.1029/91GB01778.

——, and Coauthors, 2008: Impacts of atmospheric anthropogenic nitrogen on the open ocean. *Science*, **320**, 893–897, doi:10.1126/science.1150369.

ECMWF, 2010: ERA-Interim dataset (January 1979 to present). ECMWF Data Server. Subset used: 1999–2009, accessed 1 March 2010. [Available online at http://apps.ecmwf.int/datasets/data/interim-full-daily/.]

Fomba, K. W., K. Muller, D. van Pinxteren, and H. Herrmann, 2013: Aerosol size-resolved trace metal composition in remote northern tropical Atlantic marine environment: Case study Cape Verde islands. *Atmos. Chem. Phys.*, **13**, 4801–4814, doi:10.5194/acp-13-4801-2013.

——, K. Müller, D. van Pinxteren, L. Poulain, M. van Pinxteren, and H. Herrmann, 2014: Long-term chemical characterization of tropical and marine aerosols at the Cape Verde Atmospheric Observatory (CVAO) from 2007 to 2011. *Atmos. Chem. Phys.*, **14**, 8883–8904, doi:10.5194/acp-14-8883-2014.

Ganzeveld, L., J. Lelieveld, and G.-J. Roelofs, 1998: A dry deposition parameterization of sulfur oxides in a chemistry and general circulation. *J. Geophys. Res.*, **103**, 5679–5694, doi:10.1029/97JD03077.

Helmers, E., and O. Schrems, 1995: Wet deposition of metals to the tropical North and the South Atlantic Ocean. *Atmos. Environ.*, **29**, 2475–2484, doi:10.1016/1352-2310(95)00159-V.

Jickells, T. D., and Coauthors, 2005: Global iron connections between desert dust, ocean biogeochemistry, and climate. *Science*, **308**, 67–71, doi:10.1126/science.1105959.

Johansen, A. M., R. L. Siefert, and M. R. Hoffmann, 2000: Chemical composition of aerosols collected over the tropical North Atlantic Ocean. *J. Geophys. Res.*, **105**, 15 277–15 312, doi:10.1029/2000JD900024.

Johnson, M. T., and Coauthors, 2008: Field observations of the ocean–atmosphere exchange of ammonia: Fundamental importance of temperature as revealed by a comparison of high and low latitudes. *Global Biogeochem. Cycles*, **22**, GB1019, doi:10.1029/2007GB003039.

Kaufman, Y. J., I. Koren, L. A. Remer, D. Tanré, P. Ginoux, and S. Fan, 2005: Dust transport and deposition observed from the Terra-Moderate Resolution Imaging Spectroradiometer (MODIS) spacecraft over the Atlantic Ocean. *J. Geophys. Res.*, **110**, D10S12, doi:10.1029/2003JD004436.

Kim, G., and T. M. Church, 2002: Wet deposition of trace elements and radon daughter systematics in the south and equatorial Atlantic atmosphere. *Global Biogeochem. Cycles*, **16**, 19-1–19-8, doi:10.1029/2001GB001407.

Krishnamurthy, A., J. K. Moore, C. S. Zender, and C. Luo, 2007: Effects of atmospheric inorganic nitrogen deposition on ocean biogeochemistry. *J. Geophys. Res.*, **112**, G02019, doi:10.1029/2006JG000334.

Lesworth, T., A. R. Baker, and T. Jickells, 2010: Aerosol organic nitrogen over the remote Atlantic Ocean. *Atmos. Environ.*, **44**, 1887–1893, doi:10.1016/j.atmosenv.2010.02.021.

Luo, C., N. Mahowald, N. Meskhidze, Y. Chen, R. L. Siefert, A. R. Baker, and A. Johansen, 2005: Estimation of iron solubility from observations and a global aerosol model. *J. Geophys. Res.*, **110**, D23307, doi:10.1029/2005JD006059.

Mahowald, N. M., and Coauthors, 2005: The atmospheric global dust cycle and iron inputs to the ocean. *Global Biogeochem. Cycles*, **19**, GB4025, doi:10.1029/2004GB002402.

——, and Coauthors, 2008: Global distribution of atmospheric phosphorus sources, concentrations and deposition rates, and anthropogenic impacts. *Global Biogeochem. Cycles*, **22**, GB4026, doi:10.1029/2008GB003240.

Mills, M. M., C. Ridame, M. Davey, J. La Roche, and R. J. Geider, 2004: Iron and phosphorus co-limit nitrogen fixation in the eastern tropical North Atlantic. *Nature*, **429**, 292–294, doi:10.1038/nature02550.

Moore, C. M., and Coauthors, 2009: Large-scale distribution of Atlantic nitrogen fixation controlled by iron availability. *Nat. Geosci.*, **2**, 867–871, doi:10.1038/ngeo667.

Okin, G., and Coauthors, 2011: Impacts of atmospheric nutrient deposition on marine productivity: Roles of nitrogen, phosphorus, and iron. *Global Biogeochem. Cycles*, **25**, GB2022, doi:10.1029/2010GB003858.

Prospero, J. M., and P. J. Lamb, 2003: African droughts and dust transport to the Caribbean: Climate change implications. *Science*, **302**, 1024–1027, doi:10.1126/science.1089915.

——, and Coauthors, 1996: Atmospheric deposition of nutrients to the North Atlantic Basin. *Biogeochemistry*, **35**, 27–73, doi:10.1007/BF02179824.

——, J. E. Bullard, and R. Hodgkins, 2012: High-latitude dust over the North Atlantic: Inputs from Icelandic proglacial dust storms. *Science*, **335**, 1078–1082, doi:10.1126/science.1217447.

——, F.-X. Collard, J. Molinie, and A. Jeannot, 2014: Characterizing the annual cycle of African dust transport to the Caribbean Basin and South America and its impact on the environment and air quality. *Global Biogeochem. Cycles*, **28**, 757–773, doi:10.1002/2013GB004802.

Pye, K., 1987: *Aeolian Dust and Dust Deposits.* Academic Press, 334 pp.

Real, E., and Coauthors, 2010: Cross-hemispheric transport of central African biomass burning pollutants: Implications for downwind ozone production. *Atmos. Chem. Phys.*, **10**, 3027–3046, doi:10.5194/acp-10-3027-2010.

Savoie, D. L., J. M. Prospero, and E. S. Saltzman, 1989: Non-sea-salt sulfate and nitrate in trade wind aerosols at Barbados: Evidence for long-range transport. *J. Geophys. Res.*, **94**, 5069–5080, doi:10.1029/JD094iD04p05069.

Schlosser, C., and Coauthors, 2014: Seasonal ITCZ migration dynamically controls the location of the (sub)tropical Atlantic biogeochemical divide. *Proc. Natl. Acad. Sci. USA*, **111**, 1438–1442, doi:10.1073/pnas.1318670111.

Sedwick, P. N., E. R. Sholkovitz, and T. M. Church, 2007: Impact of anthropogenic combustion emissions on the fractional solubility of aerosol iron: Evidence from the Sargasso Sea. *Geochem. Geophys. Geosyst.*, **8**, Q10Q06, doi:10.1029/2007GC001586.

Stuut, J. B., M. Zabel, V. Ratmeyer, P. Helmke, E. Schefuss, G. Lavik, and R. Schneider, 2005: Provenance of present-day eolian dust collected off NW Africa. *J. Geophys. Res.*, **110**, D04202, doi:10.1029/2004JD005161.

Sunda, W. G., 1997: Control of dissolved iron concentrations in the world ocean: A comment. *Mar. Chem.*, **57**, 169–172, doi:10.1016/S0304-4203(97)00045-5.

Ternon, E., C. Guieu, C. Ridame, S. L'Helguen, and P. Catala, 2011: Longitudinal variability of the biogeochemical role of Mediterranean aerosols in the Mediterranean Sea. *Biogeosciences*, **8**, 1067–1080, doi:10.5194/bg-8-1067-2011.

Tian, Z. L., P. Olliver, A. Veron, and T. M. Church, 2008: Atmospheric Fe deposition modes at Bermuda and the adjacent Sargasso Sea. *Geochem. Geophys. Geosyst.*, **9**, Q08007, doi:10.1029/2007GC001868.

Ussher, S., E. P. Achterberg, C. F. Powell, A. R. Baker, T. D. Jickells, R. Torres, and P. J. Worsfold, 2013: Impact of atmospheric deposition on the contrasting iron biogeochemistry of the North and South Atlantic Ocean. *Global Biogeochem. Cycles*, **27**, 1096–1107, doi:10.1002/gbc.20056.

Xie, P. P., and P. A. Arkin, 1997: Global precipitation: A 17-year monthly analysis based on gauge observations, satellite estimates, and numerical model outputs. *Bull. Amer. Meteor. Soc.*, **78**, 2539–2558, doi:10.1175/1520-0477(1997)078<2539:GPAYMA>2.0.CO;2.

Zamora, L. M., J. M. Prospero, and D. A. Hansell, 2011: Organic nitrogen in aerosols and precipitation at Barbados and Miami: Implications regarding sources, transport and deposition to the western subtropical North Atlantic. *J. Geophys. Res.*, **116**, D20309, doi:10.1029/2011JD015660.